Fibers and Polymers 2014, Vol.15, No.2, 326-333 DOI: 10.1007/s12221-014-0326-5

Mechanical and Thermal Properties of Epoxy Composites Containing Graphene Oxide and Liquid Crystalline Epoxy

Bo Qi†, Zhengkai Yuan†, Shaorong Lu*, Kuo Liu, Shanrong Li, Liping Yang, and Jinhong Yu*

Guangxi Scientific Experiment Center of Mining, Metallurgy and Environment, Key Laboratory of New Processing Technology for Nonferrous Metals and Materials, Ministry of Education, School of Material Science and Engineering, Guilin University of Technology, Guilin 541004, China

(Received May 13, 2013; Revised July 11, 2013; Accepted July 16, 2013)

Abstract: The graphene oxide (GO) sheets are chemically grafted with γ-etheroxygentrimethoxysilane (KH560) and liquid crystalline epoxy (LCE) is synthesized from 4,4'-bis(2-hydroxyhexoxy)biphenyl (BP_2) and epichlorohydrin before being incorporated into epoxy matrix. Then we present a novel approach to the fabrication of advanced polymer composites from epoxy matrix by incorporation of two modifiers, which are grafted GO (g-GO) and LCE. The mechanical properties of epoxy composites are greatly improved by incorporating LCE/g-GO hybrid fillers. For instance, the addition of 3 wt% hybrid filler (2 wt% g-GO and 1 wt% LCE) into the epoxy matrix resulted in the increases in impact strength by 132.6 %, tensile strength by 27.6 % and flexural strength by 37.5 %. Moreover, LCE/g-GO hybrid fillers are effective to increase thermal decomposition temperature, glass transition temperature, and storage modulus by strong affinity between the fillers and epoxy matrix.

Keywords: Epoxy resin, Liquid crystalline epoxy, Graphene oxide, Mechanical property, Thermal property

Introduction

Epoxy resin (EP) is a very important class of thermoset polymer used in composite industry at present. It is frequently used in demanding applications due to excellent chemical and corrosion resistance, outstanding adhesion properties, low shrinkage and low price. When cured, the highly-cross linked microstructure provides high modulus and strength, good resistance to creep, good performance at elevated temperatures but poor ductility. Toughness for cured epoxy resin is highly desirable to be improved. Many options have been used to toughen the epoxies. Incorporating rigid, or reactive rubbery particles, or both of them [1,2] into the epoxy networks is really an effect way to improve the toughness, but it is always at the expense of glass transition temperature and strength. Another way is bringing in tough, high performance and thermal stable engineering plastics in the epoxy networks, such as polyether-sulfones [3] and polyetherimides [4]. The deficit of this method is that the process molding of these engineering plastics requires high temperature. Moreover, thermotropic liquid crystalline polymers and surface modified graphite oxide with reactive groups which are able to react with hydroxyl or epoxy group is also used to improve the toughness while having little effect on other properties [5,6].

Graphene is an atomically thin, 2-dimensional network of sp^2-hybridized carbons. One of the potential applications of graphene is reinforcement for polymers. Significantly improved electrical, mechanical and gas barrier properties of graphene/polymer nanocomposites have been reported [7,8]. Liang *et al.* [9]. prepared a nanocomposite of graphene/polymer with a 76 % increase in tensile strength and a 62 % improvement of Young's modulus at a loading of 0.7 vol% graphite oxide. Wang *et al.* [10]. reported that a freestanding and flexible graphene/polyaniline composite paper gave a favorable tensile strength of 12.6 MPa. However, graphene tends to form irreversible agglomerates or even restack due to van der Waals interactions because of their high specific surface area, an effective approach in this regard is based on the chemical exfoliation of graphite to graphite oxide [11]. This material consists of graphene derived sheets, heavily oxygenated, bearing hydroxyl, epoxide, carbonyl and carboxylic functional groups [12]. This makes graphite oxide has hydrophilic and can form strong physical interactions with polymer due to various oxygen functional groups including hydroxyls, epoxides, carbonyls and carboxyls [13-15]. More importantly, the surface modification of graphene sheets is therefore necessary to ensure the sheets are homogeneously dispersed in the matrix. Some authors have reported that the thermal stability, electrical and mechanical properties of polymers could be greatly improved by the incorporation of graphite oxide nanosheets [16-20] and graphene [21,22].

Liquid crystalline epoxy (LCE) has been studied by many research groups because they has many advantages such as anisotropic orientation, high heat resistance, high mechanical properties, low coefficient of thermal expansion, low dielectric constant, and good dimensional stability [23]. As compared to neat epoxy, crosslinked LCE exhibits higher fracture toughness and mechanical properties when oriented by magnetic fields [23,24]. Recently, several of liquid crystalline epoxy monomer or polymer were synthesized, characterized and applied to acquire materials with high modulus, high

†These authors contributed equally to this study.
*Corresponding author: gllushaorong@glite.edu.cn
*Corresponding author: yujinhong@glut.edu.cn

glass transition temperature and superior toughness. Jun Yeob and co-works [25] described the synthesis and curing of liquid crystalline epoxy resins based on the biphenyl mesogenic group to prepare high heat resistant liquid crystalline networks. In addition, anisotropic mechanical properties of oriented LCE were studied by Jahromi *et al.* [26]. Among these LCE resins, aromatic ester-based LCE is promising as an advanced material because it is easy to synthesize and has a high heat resistance and excellent mechanical properties [27].

LCE polymers are also known to have the highest moduli of polymers in general. Because of the high ordering between LCE polymer chains it is of interest to determine if the GO sheets chemically grafted with γ-etheroxygentrimethoxysilane (KH560) (g-GO) would be dispersed into the LCE and epoxy resin matrix, it causes the mechanical properties to be improved. In this study, a strategy of a combination of LCE and GO for the excellent mechanical and thermal properties has been proposed. Before being incorporated into epoxy matrix, the g-GO and LCE was synthesized from 4,4'-bis(2-hydroxyhexoxy)biphenyl (BP_2) and epichlorohydrin. The LCE can react and bridge adjacent the g-GO and inhibit their aggregation, resulting in an increased contact surface area between LCE/g-GO structures and the polymer. A remarkable positive effect between LCE and g-GO on the enhanced mechanical and thermal properties of the epoxy composites was demonstrated.

Experimental

Materials

Nature flake graphite (325 mesh, 99 %) was obtained from Qingdao Hengrui Graphite Co., Ltd. China. 4,4'-dihydroxybiphenyl, 2-chloroethanol, and γ-etheroxygentrimethoxysilane (KH560), were obtained from Shanghai Chemical Reagents Company, China. The epoxy resin used in this study is diglycidylether of bisphenol A (DGEBA, E-51, epoxy value=0.51, supplied by Yueyang Chemical Plant, China, without further purification. 4,4'-diaminodiphenylsulphone (DDS) purchased from Shanghai Chemical Reagent Company, China, with a molecular mass of 248.31 and purity >96 % according to the supplier. Deionized water was used throughout the experiments.

Synthesis of the KH560 Grafted Graphene Oxide (g-GO)

GO was prepared from natural flake graphite powder by a modified Hummers method [11]. All reagents were used without further purification. In a typical synthesis, 1 g of graphite powder was placed into a mixture containing 46 m*l* of concentrated sulfuric acid and 1 g of $NaNO_3$. The resulting mixture was stirred in an ice bath for 4 h. After homogeneous dispersion of the graphite powder in the solution, $KMnO_4$ (6 g) was added slowly over 1 h to the solution in an ice bath at 0 °C. The mixture was then stirred for 6 h at 35 °C in an oil bath. After the reaction, the mixture was distilled with 92 m*l* of de-ionized water (D.I. water) and heated to 95 °C. After 15 min, the mixture was poured into 200 m*l* of D.I. water containing 20 % H_2O_2. The mixture was washed several times and purified with HCl and D.I. water, respectively. The collected graphite oxide was dispersed in D.I. water by ultrasonication to exfoliate the graphite oxide to GO, which was dried in a vacuum oven at 50 °C for 2 days. The obtained GOs had particles with average lateral dimensions of several micrometers and thicknesses of <5 nm.

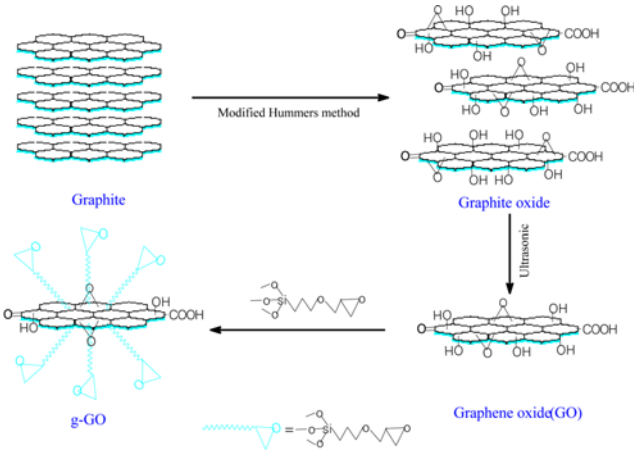

Scheme 1. The synthetic route of KH560 grafted GOs.

The g-GO was carried out in a mixture of water/ethanol (25/75 by volume). A quantity of 0.3 g of KH560 was first introduced into 100 m*l* of the mixture of water/ethanol, and temperature was kept at 80 °C. Then 1.0 g GOs were added into the above mentioned solution, and the grafting reaction was realized under sheering for 5 h at 80 °C. The reaction product was filtered and washed by using a mixture water/ethanol and dried at room temperature, the resultant product was ground and placed in a sealed container. The reaction process of KH560 grafted GOs is shown in Scheme 1.

Synthesis of LCE

A mixture of sodium hydroxide (3.20 g, 80 mmol), 4,4'-dihydroxybiphenyl (3.72 g, 20 mmol), and 80 m*l* ethanol was stirred at 70 °C for 3 min. Then, 7.25 g of 2-chloroethanol was added into the mixture. The mixture was again stirred at 80 °C for 24 h. A precipitate was collected and washed with hot alcohol. The final product was dried at 80 °C. Its molecular structure is shown step 1 in Scheme 2. A mixture of BP_2 (2.66 g, 9.71 mmol), 50 m*l* N,N'-dimethylformamide, sodium hydroxide (1.60 g, 40 mmol) and 20 m*l* deionized water was stirred at 90 °C for 1 h. Then, epichlorohydrin (10.0 g, 0.11 mol) and tetrabutylammonium bromide (0.05 g, 0.16 mmol) were added into the mixture, the mixture was again stirred at 110 °C for 6 h, and the remained epichlorohydrin was distilled under reduced pressure. After cooling, a precipitate was collected and washed with a mixture water/ethanol. The

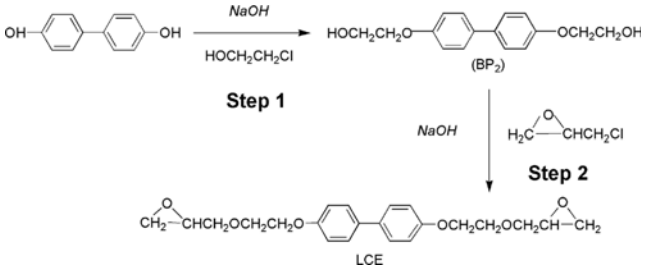

Scheme 2. Synthesis of LCE.

Table 1. Formulation of the composite (parts by weight [pbw])

Sample	Epoxy	DDS	g-GO	LCE
Neat epoxy	100	30	0	0
1 wt% epoxy	100	30	2	1
3 wt% epoxy	100	30	2	3
5 wt% epoxy	100	30	2	5
7 wt% epoxy	100	30	2	7

final product was dried at 60 °C. The synthesis route is shown step 2 in Scheme 2.

Preparation of Epoxy/LCE/g-GO Composites

A stoichiometric amount of DDS (30 g/100 g of epoxy resin) was used to prepare the epoxy/LCE/g-GO composites. LCE and g-GO with DDS was dispersed in acetone by an ultrasonicator bath for 30 min. Then the mixture was added into vacuum with a stoichiometric amount of epoxy resin and degassed at 130 °C for about 1 h. The resulting mixture was then cast into a preheat mold coated with silicone resin. All samples were cured at 120 °C for 2 h, 160 °C for 2 h and 180 °C for 2 h. The content of LCE and g-GO was calculated based on the amount of the epoxy resin. Nanocomposites containing constant weigh fraction (2 wt%) of g-GO and different weight fractions (1 %, 3 %, 5 %, and 7 %) of the LCE were prepared. The details of the composite samples are given in Table 1.

Characterization

Fourier transform infrared (FT-IR) spectra was recorded on a Perkin-Elmer 1710 spectrophotometer. Fourier transformed infrared spectrometer in the frequency range 4000-500 cm^{-1} in the attenuated total reflection mode.

The wide angle X-ray diffraction (WAXD) analysis was recorded on a type/BRUKER-AXS D8ADVANCE X-ray diffractometer equipped with a computer controller. The scanning rate was 4 °/min and the scanning scope of 2θ was 5-50 ° at room temperature.

The surface functionalization of the GO and g-GO was analyzed qualitatively by X-ray photoelectron spectroscopy (XPS) using a VG-microtech ESCA2000 spectrometer equipped with a hemispherical electron analyzer and aMgJa (hm=1.2536 keV) X-ray source.

Transmission electron microscopy (TEM) images were obtained with a TEM (Philips CM300 FEG) at an accelerating voltage of 5.0 kV. The samples for TEM observations were prepared by dropping the solutions on the copper grids.

The morphology of the fracture surfaces were observed by a scanning electron microscope (SEM: JSM-6380LV, Japan) at an accelerating voltage of 20 kV, and the surface was coated with a thin layer of carbon powder to reduce charge built up on the surface and improve conductivity.

The optical textures were obtained by a Leica DMxRP polarizing microscope.

The impact strength was measured on a tester of type XJJ-5, which is with no notch in the specimen according to China National Standard GB1043-79.The specimen was with a thickness of 4 mm and width of 10 mm and length of 80 mm. The tensile strength was examined on an electron omnipotence tester of type RGT-5.The tensile rate was 2 $mm \cdot min^{-1}$ and according to China National Standard GB1040-92. All the presented results are the average value of five specimens.

Thermogravimetric analysis (TGA) of the composites samples were performed on NETZSCH STA 449C by heating the sample from room temperature to 575 °C at a heating rate of 10 °C/min in nitrogen atmosphere.

Differential scanning calorimetry (DSC) analysis on NETZSCH DSC204 was carried out under a heating rate of 5 K/min.

Thermomechanical properties, modulus, and glass transition temperature were determined using a linear rheometer (Q800 dynamic mechanical analyzer, TA Instruments, USA) in a single cantilever bending mode, at a frequency of 1.0 Hz from 40 °C to 250 °C at a heating rate of 3 °C/min.

Results and Discussion

FT-IR Analysis

Figure 1 shows the FT-IR spectra of LCE, GO, and g-GO.

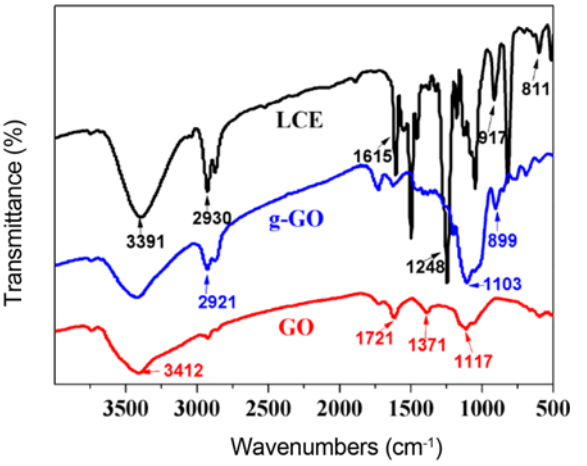

Figure 1. FT-IR spectra of LCE, GO, and g-GO.

As shown in Figure 1, a strong absorption at 3391 cm^{-1} is due to the stretching vibration of phenolic hydroxyl group. The band at 1248 cm^{-1} is associated with stretching of the C-O bond of alkoxyl ether groups. The absorptions at 811 cm^{-1}, 917 cm^{-1} are due to the epoxy group, and the band at 2930 cm^{-1} assigned to the alkyl groups. The characteristic features in the FT-IR spectrum of GO are absorption bands corresponding to C=O carboxyl 1721 cm^{-1}, the C-OH stretching at 1371 cm^{-1}, and the C-O stretching at 1117 cm^{-1}, 3412 cm^{-1} is due to the stretching vibration of hydroxyl group [28,29].

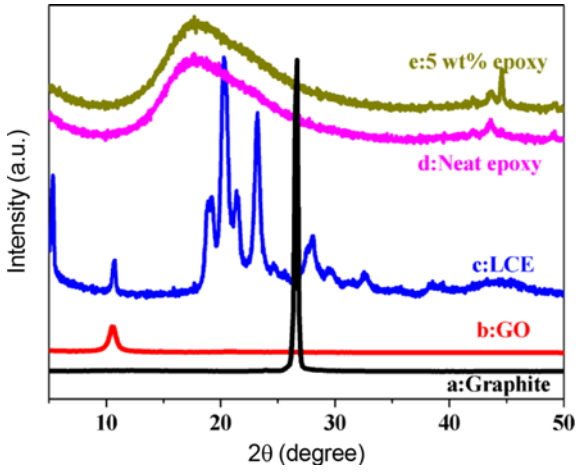

Figure 2. XRD patterns: (a) graphite, (b) GO, (c) LCE, (d) neat epoxy, and (e) 5 wt% epoxy.

After grafted KH560, as show in Figure 1, the absorptions at 899 cm^{-1} is due to the epoxy group, and the broad peak at 1103 cm^{-1} is assigned to the Si-O-C [30], the band at 2921 cm^{-1} assigned to the alkyl groups. It confirms that the surface of graphite oxide was successfully grafted by KH560.

WAXD Analysis

The wide X-ray diffractograms of graphite, GO, LCE, neat epoxy and 5 wt% epoxy composite was shown in Figure 2. The strong and sharp diffraction peak of natural graphite (Figure 2(a)) appears at about 26.6°. This is the characteristic peak of hexagonal graphite with a *d*-spacing of 0.34 nm. Upon conversion of graphite into GO. The peak position shifts to 10.7° (Figure 2(b)) and the interlayer spacing increases to 0.84 nm. This increase of the *d*-spacing is due to the intercalation of -OH containing functional groups in between graphene layers [31,32]. The curve for LCE (Figure 2(c)) shows a group of sharp diffraction peaks in the 2θ region of 10.5-32.4° corresponding to the *d*-spacing range. It illustrates that there are some crystallite structure in LCE except amorphous phase. However, the curve for 5 wt% epoxy composite (Figure 2(e)) doesn't show any sharp diffraction peaks except for the broad peaks. This is because that LCE/g-GO was dissolved in the epoxy matrix in advance or completely separated by epoxy resin cross-linking networks, so the crystallite phase disappeared and the *d*-spacing of epoxy/LCE/g-GO composite is closed to the neat epoxy resin (Figure 2(d)).

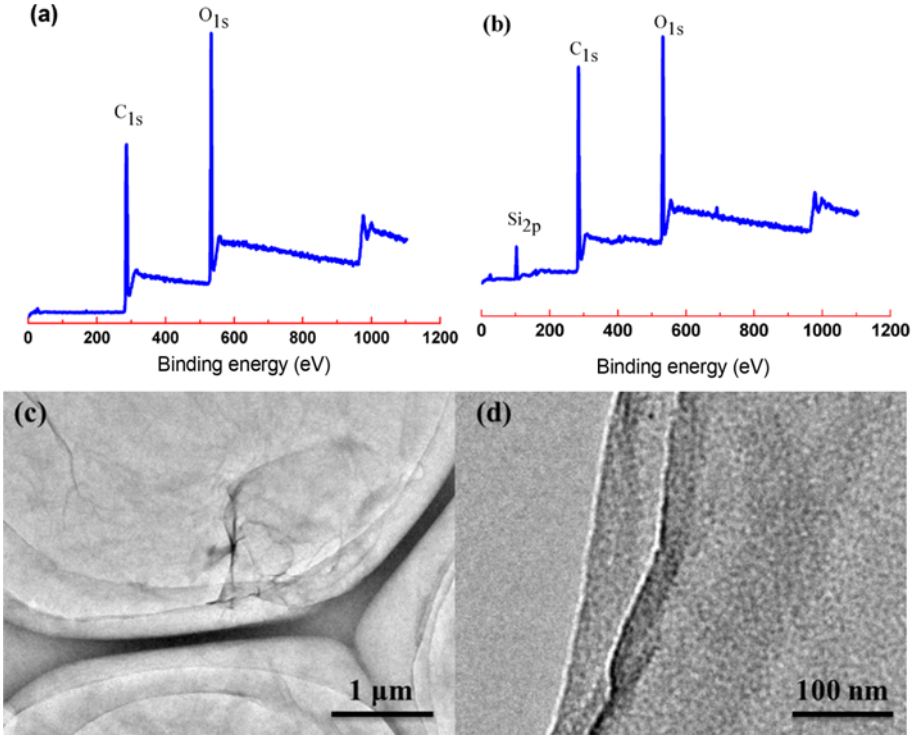

Figure 3. XPS survey spectra of (a) GO and (b) g-GO, TEM images of (c) GO and (d) g-GO.

XPS and TEM Analysis

XPS analysis was used to verify the surface composition of the GO nanosheet and detect the functional groups on the nanosheet based on chemical shift observations. The results of the XPS survey spectra are presented in Figure 3(a) and 3(b). Figure 3(a) and 3(b) shows wide scan spectra in the range of 0-1,200 eV used to identify the surface elements present with quantitative analysis. In both the GO and g-GO spectra, C_{ls} and O_{1s} signals appear at 286 and 530 eV, respectively. After grafted the silane agent onto the GO, g-GO shows a new Si_{2p} peak at 101 eV. A detailed analysis of the XPS spectra presented clear evidence that the GO was chemically modified by silane agent. TEM were further used to investigate the morphology and microstructure of GO and g-GO. As shown in Figure 3(c), GO sheets exhibit a wrinkled and folded structure of several micrometres, but the surface of the GO sheets is fairly smooth. It is well known that the surface of GO is negatively charged over the 2-11 pH range, which originates from the ionization of the carboxylic acid and phenolic hydroxy groups. When the GO solution was dropped on the grids, the GO sheets were likely to experience both electrostatic repulsion and van der Waals attraction during the solvent evaporation process. On the other hand, the residual π-conjugated domains can also contribute to the attraction between GO sheets. These two opposite forces make GO nanosheets tend to congregate together to form multilayer agglomerates. The individual nanosheets have sizes extending from tens to several hundreds of square nanometers. When compared with GO, the surface of g-GO nanosheets appear to be rough and clearly covered by the addends, which are attributed to the grafting of silane agent, as shown in Figure 3(d).

Thermal and Phase Behavior of LCE

The liquid crystalline phase behavior of LCE was observed by a Leica polarized optical microscope (POM) equipped with the heating stage. As LCE was heated to 160 °C, a nematic texture was observed. The representative sample of the POM taken at 175 °C was displayed in Figure 4. While being consecutively heated to 190 °C, the nematic texture disappeared. The temperature region of the nematic liquid crystalline phase obtained from POM is agreement with the result of DSC measurement in Figure 5. The crystalline melting temperature (*Tm*) of the LCE sample was 159.6 °C and its isotropic temperature (or clearing temperature, *Ti*) was approximate 189.3 °C. LCE exhibits a nematic mesophase between 159 °C and 189 °C. The phase behaviour of the LCE sample is shown in Figure 5. The two endothermic peaks are ascribed to the crystalline-nematic and nematic-isotropic phase transitions in the order of increasing temperature.

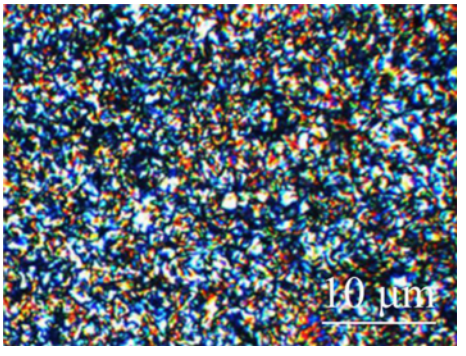

Figure 4. Representative POM of the texture of LCE (at 175 °C, magnification: 200×).

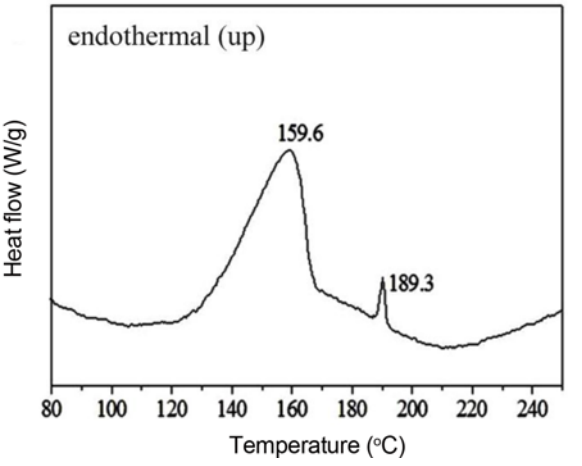

Figure 5. The DSC curve of LCE.

Morphology of Composites

Scanning electron microscopic (SEM) micrographs of neat epoxy and epoxy resin/LCE/g-GO composite specimens were considered for failure surface. In Figure 6(a), the fracture surface of the neat epoxy specimen showing the river-like fracture surface, this is indicative of brittle material fracture surface morphology. The relatively smooth surface indicates little resistance was needed for crack propagation. Figure 6(b-e) shows the roughness of a fracture surface of epoxy resin/LCE/g-GO composites specimen. The roughness on the surface indicates that a comparatively higher amount of impact energy was required for the crack to propagate. From the figure, it is seen that the non-uniformly dispersed and non-netted structures formed in different orientations, which can disperse stress, indicating the characteristic of toughening fracture. The similar result has been shown by various authors that the liquid crystalline domain structure causes an increase in fracture toughness for liquid crystalline epoxy resin [33]. However, with the LCE/g-GO loading increasing, large g-GO agglomerates were clearly seen from the sample and numerous micro voids existed between g-GO nanosheets in the epoxy composites, as shown in Figure 6(c-e). The agglomerates present in LCE/g-GO composites caused easier crack initiation and propagation, and the poor g-GO dispersion leads to the mechanical properties of epoxy/LCE/g-GO composites decreased.

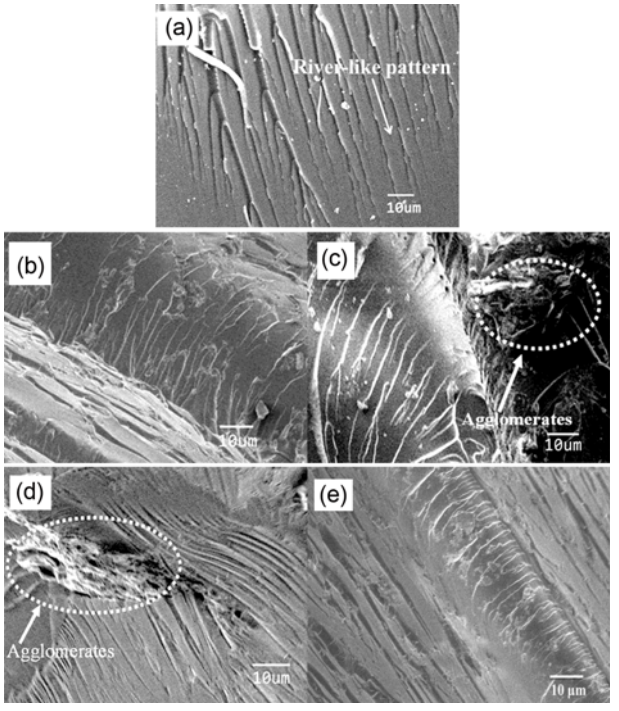

Figure 6. SEM images of the impact fracture surfaces of (a) neat epoxy, (b) 1 wt% epoxy, (c) 3 wt% epoxy, (d) 5 wt% epoxy, and (e) 7 wt% epoxy.

Mechanical Properties

The general purpose of incorporating a small amount of LCE/g-GO into the epoxy matrix is to improve its mechanical properties. The mechanical properties of neat epoxy and epoxy/LCE/g-GO composites are summarized in Table 2. From this table, it can be seen that all epoxy/LCE/g-GO composites show higher impact strength, flexural strength, tensile strength and modulus than the neat epoxy curing system. For example, the addition of 3 wt% hybrid filler (2 wt% g-GO and 1 wt% LCE) into the matrix resulted in the increases in impact strength by 132.6 %, tensile strength by 27.6 % and flexural strength by 37.5 % from the neat epoxy sample, respectively. At the highest loading (2 wt% g-GO and 7 wt% LCE) of LCE/g-GO hybrid filler used in this study, impact strength, tensile strength and flexural strength of epoxy composite are 25.7 kJ/m^2, 63.2 MPa, and 122.9 MPa, respectively. All these values were higher than that of the neat epoxy sample. Meanwhile, tensile modulus for all epoxy composites reached the maximum at 5 wt% hybrid filler (2 wt% g-GO and 3 wt% LCE), then decreased with increasing hybrid filler, indicating a well-known negative effect of numerous micro voids on the modulus of filler/polymer composites due to the LCE fillers are agglomerate. This result may be explained by the fact that the agglomerates in higher LCE/g-GO contents composites act as large particles. These agglomerates trap polymer in the void space between LCE and g-GO, and effectively reduce the volume fraction of the epoxy matrix, similar results have been reported in the literature [33,34]. However, it is interesting to note that although the tensile modulus decreased from the maximum (1123.4 MPa) at 5 wt% hybrid filler to 1045.8 MPa, the value of epoxy composite is still higher than that (1029.0 MPa) of the neat epoxy. The enhanced modulus of epoxy by adding the LCE/g-GO hybrid fillers is considered to be due to the strong interfacial adhesion between the LCE/g-GO hybrid and epoxy matrix. The results of modulus are well supported for that the interfacial modification of GOs plays an important role in the composite to enhance the mechanical properties, which are agreement with the previous studies [35-37].

Thermal Properties

Thermogravimetric analysis (*TGA*) was applied to evaluate the thermal stability of the epoxy/LCE/g-GO composites. The *TGA* curves of the neat epoxy and its composites with different LCE/g-GO content are shown in Figure 7. One could see that all the *TGA* curves displayed one-step degradation mechanism, suggesting that the existence of LCE/g-GO did not significantly alter the degradation mechanism of the matrix polymers. For the neat epoxy, the initial decomposition occurred at 372 ^{o}C, while the epoxy/LCE/g-GO composite was 382 ^{o}C when LCE/g-GO hybrid filler content is 7 wt%. The results indicate that the composites would become highly crosslinked with increasing the content of LCE/g-GO, and the thermal weight loss of the composites decrease with increasing the LCE/g-GO content. At the temperature of 700 ^{o}C, the char yield of neat epoxy is 15 wt% and that of the composite (LCE/g-GO content 7 wt%) is 26 wt%. Consequently, the thermal stability of epoxy/LCE/g-GO composites is higher than that of neat epoxy at high temperature.

Table 2. Mechanical properties of the different contents of LCE/g-GO modified epoxy resin

Sample	Impact strength (kJ/m^2)	Tensile strength (MPa)	Tensile modulus (MPa)	Flexural strength (MPa)
Neat epoxy	17.5(0.55)	59.4(0.48)	1029.0(0.38)	79.5(0.51)
1 wt% epoxy	36.6(0.46)	68.2(0.46)	1089.4(0.40)	109.3(0.48)
3 wt% epoxy	40.7(0.53)	75.8(0.41)	1118.6(0.36)	121.9(0.47)
5 wt% epoxy	31.5(0.48)	61.9(0.48)	1123.4(0.32)	130.6(0.45)
7 wt% epoxy	25.7(0.45)	63.2(0.50)	1045.8(0.35)	122.9(0.42)

Values in bracket are the standard deviation of the results.

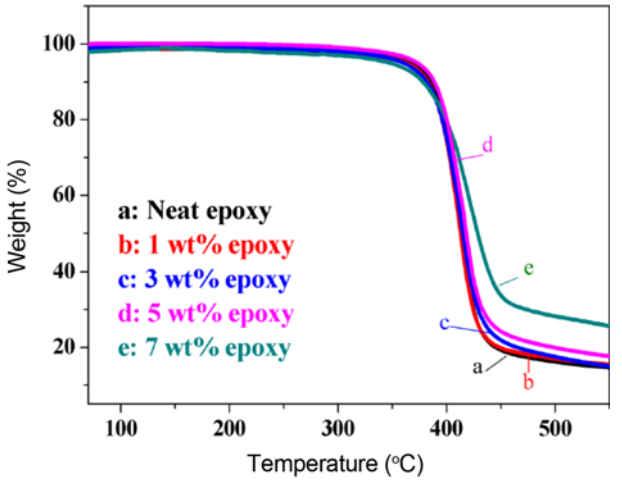

Figure 7. TGA curves of the neat epoxy and its composites.

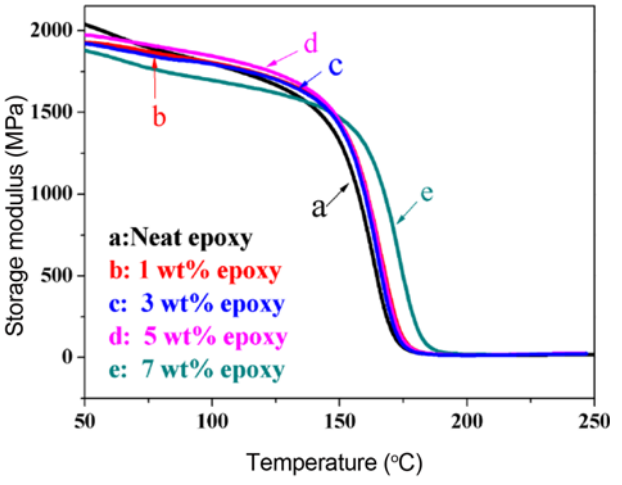

Figure 8. Storage modulus curves for the neat epoxy and its composites.

The thermomechanical properties of composites were measured by a TA DMA Q800 at 1 Hz frequency. Figure 8 shows the variation of storage modulus as a function of temperature for neat epoxy and its composites. Obviously, all the composites exhibit temperature dependences similar to the neat epoxy. As the temperature increased, both neat epoxy and its composites showed a gradual drop in storage modulus followed by a sudden drop at the glass transition temperature (*Tg*). The drop in modulus is related to the material transition from a glassy state to a rubbery state. As shown in the Figure 8, a higher storage modulus with the higher LCE content was also observed in the rubbery region. At 160 °C, the 5 wt% epoxy composites showed about 40 % higher storage modulus than that of the neat epoxy. This suggests the interaction between LCE/g-GO and the epoxy matrix improved, which hindered the matrix chains mobility near LCE/g-GO surface.

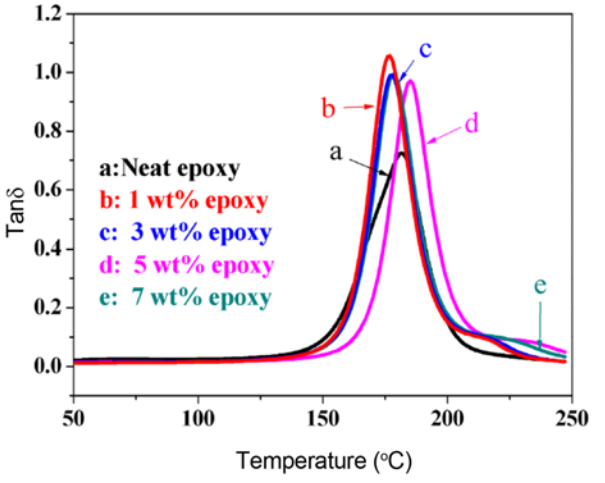

Figure 9. Loss factor versus temperature for the neat epoxy and its composites.

Figure 9 shows the changes of loss factor (Tan δ) with variation of temperature for different specimens. From the Figure, it can be seen that the glass transition temperature of neat epoxy increased slightly with the incorporation of g-GO/LCE. The *Tg*s were 174 °C, 179 °C, 184 °C and 180 °C for g-GO/LCE contents of 1 wt%, 3 wt%, 5 wt%, and 7 wt%, respectively. Since *Tg* reflects the mobility level of polymer segments in chain/networks in the matrix, and an increase in *Tg* corresponds to a decrease in mobility of the polymer networks [38,39]. Several reasons are probably ascribed to the above phenomena. First, for the epoxy composites with the good dispersed g-GO and thus results in a slight enhancement in Tg value compare with the neat epoxy. Second, the LCE are agglomerate and thicker, resulting in a decrease of the surface area in contact with the polymer and a smaller Tg shift with the increase of LCE loading. This reason can well explain that the *Tg* of composites with 5 wt% LCE is higher than that of composite with 7 wt% LCE. In general, the increase in *Tg* is attributed to the good adhesion between the polymer and the reinforced particles so that the nanometer size particles can restrict the segmental motion of cross-links under loading [40-42]. Moreover, the reduction of Tan δ indicates significantly hindered motion of matrix chains.

Conclusion

A new type of epoxy/LCE/g-GO composites was developed using LCE/g-GO as hybrid filler reinforcing agent. The mechanical properties, fracture behaviours, thermal properties and dynamic mechanical behavior of composites were systematically investigated. SEM images showed that the LCE/g-GO was dispersed well when LCE/g-GO loading was lower, but the aggregations formed with the increasing content of hybrid LCE/g-GO. The mechanical properties

testing showed that the incorporation of LCE/g-GO improved the impact strength, tensile strength and flexural strength of composites. For example, the addition of 3 wt% hybrid filler (2 wt% g-GO and 1 wt% LCE) into the matrix resulted in the increases in impact strength by 132.6 %, tensile strength by 27.6 % and flexural strength by 37.5 %, respectively. Meanwhile, *TGA* and *DMA* results showed that the epoxy/LCE/g-GO composites exhibited higher thermal stability and glass transition temperature than that of the neat epoxy. The glass transition temperature of neat epoxy was increased from 174 to 184 ^{o}C at 5 wt% LCE/g-GO.

Acknowledgements

The authors are grateful for the financial support by the National Natural Science Foundation of China (51163004 and 51303034), the Natural Science Foundation of Guangxi Province, China (No. 2013GXNSFAA019308), the Scientific Research and Technology Development Plan of Guangxi Province of China (Nos.1298025-8; 0992022-4) and Inovation Team of Guangxi Universities' Talent Highland.

References

1. R. J. Day, P. A. Lovell, and A. A. Wazzan, *Compos. Sci. Technol.*, **61**, 41 (2001).
2. J. Jiao, X. Sun, and T. J. Pinnavaia, *Polymer*, **50**, 983 (2009).
3. S. Alessi, D. Conduruta, G. Pitarresi, C. Dispenza, and G. Spadaro, *Polym. Degrad. Stab*., **95**, 677 (2010).
4. C. C. Riccardi, J. Borrajo, R. J. J. Williams, E. Girard-Reydet, H. Sautereau, and J. P. Pascault, *J. Polym. Sci. Pol. Phys.*, **34**, 349 (1996).
5. C. L. Bao, Y. Q. Guo, L. Song, Y. C. Kan, X. D. Qian, and Y. Hu, *J. Mater. Chem.*, **21**, 13290 (2011).
6. S. H. Che, S. C. Thickett, M. R. Whittaker, and P. B. Zetterlund, *J. Polym. Sci. Pol. Chem*., **51**, 47 (2013).
7. H. Kim and C. W. Macosko, *Polymer*, **50**, 3797 (2009).
8. T. Kuilla, S. Bhadra, D. Yao, N. H. Kim, S. Bose, and J. H. Lee, *Prog. Polym. Sci*., **35**, 1350 (2010).
9. J. Liang, Y. Huang, L. Zhang, Y. Wang, Y. Ma, and T. Guo, *Adv. Funct. Mater*., **19**, 2297 (2009).
10. Z. M. Dang, J. K. Yuan, J. W. Zha, T. Zhou, S. T. Li, and G. H. Hu, *Prog. Mater. Sci.*, **57**, 660 (2012).
11. L. Cui, J. Liu, R. Wang, Z. Liu, and W. Yang, *J. Polym. Sci. Pol. Chem*., **50**, 4423 (2012).
12. H. Kang, A. Kulkarni, S. Stankovich, R. S. Ruoff, and S. Baik, *Carbon*, **47**, 1520 (2009).
13. L. Madaleno, R. Pyrz, A. Crosky, L. R. Jensen, J. C. M. Rauhe, and V. Dolomanova, *Compos. Part A-Appl. S*, **44**, 1 (2013).
14. M. A. Rafiee, J. Rafiee, Z. Wang, H. H. Song, Z. Z. Yu, and N. Koratkar, *ACS Nano*, **3**, 3884 (2009).
15. Y. Matsuo, Y. Nishino, T. Fukutsuka, and Y. Sugie, *Carbon*, **45**, 1384 (2007).
16. R. Li, C. Liu, and J. Ma, *Carbohyd. Polym*., **84**, 631 (2011).
17. R. Ma and T. Sasaki, *Adv. Mater.*, **22**, 5082 (2010).
18. Y. Zhou, F. Pervin, V. K. Rangari, and S. Jeelani, *Mater. Sci. Eng. A*, **426**, 221 (2006).
19. N. Y. Yuan, F. F. Ma, Y. Fan, Y. B. Liu, and J. N. Ding, *Compos. Part A*, **43**, 2183 (2012).
20. J. An, G. W. Jeon, and Y. G. Jeong, *Fiber. Polym.*, **13**, 507 (2012).
21. J. Yu, X. Huang, C. Wu, and P. Jiang, *IEEE Trans. Dielectr. Electric. Insul*., **18**, 478 (2011).
22. J. Yu, P. Jiang, C. Wu, L. Wang, and X. Wu, *Polym. Compos.*, **32**, 1483 (2011).
23. Y. L. Liu, Z. Q. Cai, X. Wen, P. Pi, D. Zheng, and J. Cheng, *Thermochim. Acta*, **513**, 88 (2011).
24. M. Harada, N. Okamoto, and M. Ochi, *J. Polym. Sci. Pol. Phys.*, **48**, 2337 (2010).
25. A.Jannesari, S. R. Ghaffarian, N. Mohammadi, F. A. Taromi, and A. Molaei, *Thermochim. Acta*, **425**, 91 (2005).
26. S. Jahromi, J. Lub, and G. N. Mol, *Polymer*, **35**, 622 (1994).
27. R. N. Jana and J. W. Cho, *Fiber. Polym*., **10**, 569 (2009).
28. Z. Gu, C. Li, G. Wang, L. Zhang, X. Li, and W. Wang, *J. Polym. Sci. Pol. Phys*., **48**, 1329 (2010).
29. D. J. Liaw, K. L. Wang, Y. C. Huang, K. R. Lee, J. Y. Lai, and C. S. Ha, *Prog. Polym. Sci*., **37**, 907 (2012).
30. S. R. Lu, H. L. Zhang, C. X. Zhao, and X. Y. Wang, *Polymer*, **46**, 10484 (2005).
31. X. J. Shen, Y. Liu, H. M. Xiao, Q. P. Feng, Z. Z. Yu, and S. Y. Fu, *Compos. Sci. Technol.,* **72**, 1581 (2012).
32. M. Veerapandian, M. H. Lee, K. Krishnamoorthy, and K. Yun, *Carbon*, **50**, 4228 (2012).
33. Y. Zhan, X. Yang, F. Meng, J. Wei, R. Zhao, and X. Liu, *J. Colloid Interface Sci.*, **363**, 98 (2011).
34. Z. Y. Liu, S. J. Xu, B. L. Xiao, P. Xue, W. G. Wang, and Z. Y. Ma, *Compos. Part A-Appl. S.*, **43**, 2161 (2012).
35. X. Q. Su, G. Wang, W. L. Li, J. B. Bai, and H. Wang, *Adv. Powder Technol.*, **24**, 317 (2013).
36. A. Dichiara, J. K. Yuan, S. H. Yao, A. Sylvestre, and J. B. Bai, *J. Nanosci. Nanotechnol*., **12**, 6935 (2012).
37. W. K. Li, A. Dichiara, and J. B. Bai, *Compos. Sci. Technol.*, **74**, 221 (2013).
38. A. Yasmin and I. M. Daniel, *Polymer*, **45**, 8211 (2004).
39. J. H. Zhu, S. Y. Wei, N. Haldolaarachchige, D. P. Young, and Z. H. Guo, *J. Phys. Chem. C*, **115**, 15304 (2011).
40. K. P. Sau, T. K. Chaki, and D. Khastgir, *Compos. Part A-Appl. S.*, **29**, 363 (1998).
41. L. C. Tang, Y. J. Wan, D. Yan, Y. B. Pei, L. Zhao, Y. B. Li, L. B. Wu, J. X. Jiang, and G. Q. Lai, *Carbon*, **60**, 16 (2013).
42. Y. J. Wan, L. C. Tang, D. Yan, L. Zhao, Y. B. Li, L. B. Wu, J. X. Jiang, and G. Q. Lai, *Compos. Sci. Technol.*, **82**, 60 (2013).